Applied Catalysis A, General 613 (2021) 118022

Contents lists available at ScienceDirect

Applied Catalysis A, General

journal homepage: www.elsevier.com/locate/apcata

Highly tunable selectivity to benzaldehyde over Pd/ZrO_2 catalysts in Oppenauer oxidation of benzyl alcohol using acetone as H-acceptor

Christianah Aarinola Akinnawo, Dimakatso Jeannett Maheso, Ndzondelelo Bingwa, Reinout Meijboom *

Research Centre for Synthesis and Catalysis, Department of Chemical Sciences, University of Johannesburg, P. O. Box 524, Auckland Park, Johannesburg 2006, South Africa

ARTICLE INFO

Keywords:
Mesoporous zirconia
Pd nanoparticles
Oppenauer oxidation
Acid-base sites
Selectivity
Aldol condensation

ABSTRACT

The development of novel bifunctional catalysts with high selectivity is the key to achieving the goals of sustainable chemical synthesis. Here, we report the synthesis of mesoporous zirconia and transition metal-doped zirconia by inverse micelle approach. Also, meso-zirconia supported Pd nanocatalysts *via* the deposition-precipitation method. Highly crystalline Pd/ZrO_2 nanoparticles were formed, as evidenced in the pXRD and TEM analyses. The acid-base quantification was investigated using TPD-NH_3 and TPD-CO_2. Interestingly, the integration of the intrinsic chemical properties of the multi-component catalyst is significant in tailoring the catalytic activities. Interactions between the adsorbates and the moderate acid-base pair sites rather than a single dominating acid or base site mediate the higher selectivity for the aldehyde product. The 100 % chemoselectivity to benzaldehyde is ascribed to the strong synergy between Pd-Zr, which generated the moderate acid-base property. The Pd/ZrO_2 is reusable, with selectivity retained after ten cycles.

1. Introduction

The synthesis of aromatic aldehydes from selective oxidation of benzyl alcohol is one of the most valuable synthetic processes highly significant in the chemical industries as well as in academia [1]. Aldehydes are important intermediates in the synthesis of cosmetics, food flavors, pharmaceuticals, agrochemicals, plastic additives, and dyestuffs [2,3]. Diverse methods of oxidation of benzyl alcohol have been recommended; nevertheless, conventional methods involving the addition of stoichiometric amounts of heavy metal reagents, expensive and toxic oxidants are widely used. The synthetic process also involves the use of solvents that are harmful to the environment. Moreover, such a chemical transformation involves high temperature and pressure. Also, in the process, unwanted by-products are generated in large quantities [4,5].

From the perspective of environmental sustainability and process economy, it is more desirable to oxidize alcohol utilizing reagents that are cheaper, less toxic, and environmentally friendlier than their conventional counterparts such as permanganate, dichromate, and hypochlorites [6,7]. Conversely, environmentally friendly catalytic oxidation methods have been developed including aerobic oxidation protocols over transition metal catalysts. Despite its environmental and economic importance, the challenge is that it requires additives, the use of expensive noble metal catalysts, high temperature, and pressure [8]. Hence, there is a need for improvement of an alternative facile route for the oxidative transformation of $-CH_2-OH$ into $-CH=O$ under mild reaction conditions.

An alternative to aerobic oxidation is the chemoselective oxidation of alcohols that employs sacrificial carbonyl compound such as acetone as a hydrogen acceptor, through a reaction mechanism termed Oppenauer oxidation [9]. The Oppenauer oxidation is the inverse of the Meerwein-Ponndorf-Verley (MPV) reduction [10]. The mechanism is predominantly *via* elimination and addition of hydride ion between the alcoholate and the carbonyl compound. The mechanism proceeds over a six-membered cyclic transition state which is regarded as the rate-determining step (Scheme 1). Acetone, a cheap and readily available commercial solvent is still regarded as less toxic when compared to other oxidants such as permanganate, dichromate, and hypochlorites [11]. From both the environmental and economical point of view, the Oppenauer oxidation of alcohols in acetone is very appealing [12]. Several studies on these processes reported the use of homogeneous catalytic systems; however, they require stoichiometric amounts of base or acid additives, extensive synthesis of ligands, suffer from air

* Corresponding author.
E-mail address: rmeijboom@uj.ac.za (R. Meijboom).

https://doi.org/10.1016/j.apcata.2021.118022
Received 12 August 2020; Received in revised form 21 January 2021; Accepted 25 January 2021
Available online 29 January 2021

sensitivity, and are difficult to separate and reuse [13]. The aluminum alkoxide catalyst conventionally employed in this synthetic process suffers low reactivity and deactivation due to difficult separation from the homogeneous reaction mixture [10]. Hence, there is a need for the development of a highly stable and more efficient heterogeneous catalytic system to circumvent some of the inherent challenges that confront the homogeneous system.

Several reports on the utilization of solid solution (multicomponent material exhibiting a single crystal phase of the host metal oxide) of mesoporous zirconia-based catalysts in aldehyde production from catalytic oxidation of benzyl alcohol have been reported [9,14,15]. However, the efficacy of cation dopants in the crystal lattice of ZrO_2 in Oppenauer oxidation is sparsely reported. Generally, metal-doped oxides exhibit improved catalytic activity compared to their undoped counterparts due to their enhanced intrinsic properties [16]. The incorporation of cations into the zirconia lattice possibly leads to some crystal defects, depending on the valence electron difference between the dopant and the host oxide. The high energy defects lead to the generation of active sites, which in turn serve as activation sites for the reacting species at the molecular level on the surface of the catalyst. Also, the selectivity of such catalysts could be promoted by depositing metal nanoparticles on the surface [17]. The strong metal-support interaction facilitates enhanced electron density for desirable activation of the substrate molecules.

Palladium nanoparticles have been widely reported to be highly active in the selective oxidation of benzyl alcohol to benzaldehyde, this has prompted various recent research reports on Pd-based catalysts [1, 18]. Luque *et al.* [19] employed Fe doped SBA-15 supported Pd NPs in aerobic benzyl alcohol oxidation. They observed conversions higher than 80 % and high selectivity to benzaldehyde. The Pd NPs supported on nitrogen-doped carbon nanotubes Pd/N-CNT developed by Wang et al. [20] gave 90 % selectivity to benzaldehyde in aerobic oxidation of benzyl alcohol. Nevertheless, the support plays a key role in increasing palladium dispersion as demonstrated in the report by Parlett et al. [21] Zirconia is shown to be promising support for Pd NPs with excellent catalytic activity for ethylene glycol electro-oxidation [22]. The stability of the active Pd sites is crucial for selective alcohol oxidation [1].

Furthermore, the design and development of novel multicomponent catalysts with high activity and selectivity, specifically the latter, is the key to achieving the goals of green chemical synthesis. Moreover, the increasing emphasis on the improvements in the atomic efficiency of the feedstocks and the need for making chemical reactions green, demand more attention to the design and development of highly selective catalysts [18,23,24]. Among the reported research on catalytic dehydrogenation of benzyl alcohol *via* Oppenauer oxidation, only a few directed efforts to the systematic suppression of side products and tuning the selectivity for aldehyde only over Pd supported Zr-based catalysts. This prompts us to systematically investigate the key role(s) influencing the selective Oppenauer oxidation of benzylic alcohols to unsaturated aldehydes, as this is relevant commercially in industrial chemical processes.

In this contribution, we report the design of pure and metal (M = Mn, Ni, Fe, and Ce) doped zirconia catalysts using a sol-gel, inverse micelle approach. Also, Pd nanoparticles were deposited on mesoporous zirconia and dopant modified zirconia using the deposition precipitation method. To the best of our knowledge, this paper presents the first application of Pd NPs supported on mesoporous ZrO_2 in Oppenauer oxidation of benzyl alcohol. The synergistic effect of the metal-Zr interaction on the product distribution in catalytic Oppenauer oxidation of benzyl alcohol with acetone under mild reaction conditions is reported. Preliminary investigation of the Oppenauer oxidation operating parameters was achieved over pure zirconia. The optimized parameters were utilized in the catalytic evaluation of the as-prepared catalysts. Two possible reaction pathways were evident: transfer dehydrogenation of benzyl alcohol for benzaldehyde production and aldol condensation of acetone. The selectivity to either benzaldehyde or aldol products is discussed in terms of tailored concentration of Lewis acid and base sites on the zirconia catalysts, as a consequence of the synergy between the Pd-ZrO_2, CeO_2-ZrO_2 interface, and Pd-Zr, Pd-Ce, Ce-Zr intermetallic alloy active sites. Our results reveal that the Pd-ZrO_2 could be a promising catalyst for Oppenauer oxidation processes in the view of stability and effectiveness.

2. Experimental section

2.1. Materials

All reagents purchased were used without further purification. Milli Q (18 MΩ cm) water was used in the preparation of aqueous solutions. The 1-butanol (99.8 %), poly(ethylene glycol)-block-poly(propylene glycol)-block-poly(ethylene glycol) (Pluronic P-123 or PEO20-PPO70-PEO20), zirconium(IV) butoxide solution (80 % in 1-butanol), nickel (II) nitrate hexahydrate (99 %), manganese(II) nitrate tetrahydrate (97 %), cerium(III) nitrate hexahydrate (99 %), tetraethoxysilane (99 %), decane (99 %), and benzyl alcohol (99.8 %) were purchased from Sigma-Aldrich. Palladium acetate (47 %) and iron(III) nitrate nonahydrate were purchased from Sisco Research Laboratories (SRL) Pty Ltd, India, anhydrous acetone (99.5 %) from Glassworld South Africa. Chromium (III) nitrate nonahydrate (98 %) was purchased from UNIVAR, SAAR CHEM pty. Nitric acid (HNO_3) (69–70 %) was purchased from Rochelle Chemicals (RSA).

2.2. Catalysts synthesis

2.2.1. Synthesis of mesoporous zirconia-based catalysts

The surfactant-assisted, inverse micelles protocol detailed in [26] was used in the preparation of pure ZrO_2. In a typical synthesis, 0.040 mol of zirconium butoxide was dissolved in a solution containing 0.336 mol 1-butanol, 6.8×10^{-4} mol P-123, and 0.064 mol HNO_3. The solution was covered with a parafilm M and stirred for 24 h at room temperature. The 1-butanol was removed through evaporation in an oven at 120 °C for 4 h. After evaporation, calcination of the obtained yellow glassy thin flakes directly to 350 °C for 5 h at a 2 °C min heating rate was performed. The metal-doped zirconia was prepared by adding the required amount of dopant precursor with zirconium butoxide (1:4 M ratio) into the P-123 acidic solution. Thereafter, the resulting solution was thermally treated as that of the pure ZrO_2. The samples are represented as M_ZrO_2, M = metal dopant.

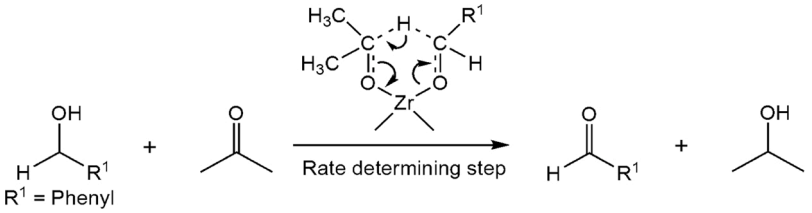

Scheme 1. Oppenauer oxidation mechanism over heterogeneous zirconia system [25].

2.2.2. Deposition of Pd nanoparticles

The Pd nanoparticles were deposited on the various mesoporous supports (SiO_2, pure and metal-doped ZrO_2) by a deposition-precipitation method. An aqueous solution of palladium acetate (0.086 g in 10 mL deionized water) was added dropwise into a 100 mL aqueous suspension containing 2 g of the support. Then heated at 80 °C for 1 h after urea addition. After stirring at 80 °C for 1 h, it was allowed to cool to room temperature, and 10 M excess of $NaBH_4$ was added dropwise to the metal-support suspension and allowed to stir for 18 h. The suspension was washed thrice with an excess amount of deionized water and separated by centrifugation at 4500 rpm for 0.5 h. The supported Pd catalyst was dried in a vacuum oven at 70 °C overnight.

2.3. Characterization of prepared catalysts

The strength and concentration of both the acid and base sites on the samples were examined using temperature-programmed desorption (NH_3- and CO_2-TPD) methods on a Micromeritics AutoChem II chemisorption analyzer. The catalyst, approximately 0.4 g was loaded in a quartz tube reactor and pretreated in helium gas flow at 200 °C for 1 h (50 mL min^{-1}) before the experiment. A mixture of NH_3/He or CO_2/He in the ratio of 1:9 was used for the measurement in the temperature range of 30−550 °C at a ramping rate of 10 °C min^{-1} or 3 °C min^{-1}, respectively. The measured flow rate for NH_3-TPD and CO_2-TPD was 25 mL STP min^{-1} and 50 mL STP min^{-1}, respectively.

The sample (10 mg) was dispersed in 1 mL methanol and sonicated for 1 h, then a drop of the suspension was placed onto a carbon-coated Cu grid. The images were captured on a JEOL Jem-2100 F transmission electron microscope (TEM) operating with an accelerating voltage of 200 kV. The particle sizes of the Pd supported catalysts were evaluated using the ImageJ software and size distribution curve.

The samples for the scanning electron microscope (SEM) were carbon-coated in an Agar Turbo carbon coater before analysis. The prepared samples were captured on a Tescan Vega 3 LMH Scanning electron microscope (SEM) using a scattering electron detector with a voltage of 20.0 kV. The distribution of the metal species was identified by elemental mapping on SEM. The metal M^{n+} component of the prepared catalysts and their corresponding weight percentage were verified with Oxford energy-disperse X-ray spectroscopy EDXS. Also, the Pd loading (wt%) in the catalytic samples was determined using the Spectro Acros ICP-OES instrument.

The nitrogen sorption experiments were performed on a Micrometrics ASAP 2460 sorption system to study the BET surface area and pore structure. The samples were degassed at 100 °C under nitrogen for 18 h and under vacuum for 10 h at the same temperature before the experiments for the removal of any physisorbed moisture. The surface areas were calculated using the Brunauer-Emmett-Teller (BET) method.

The X-ray powder diffraction (pXRD) patterns were collected on a Rigaku SmartLab diffractometer system operating with Cu Kα1 radiation (λ =1.5406 Å) at 25 °C. The 2θ diffraction patterns measurement was taken in the range 5−90° angle with a step of 0.020°. The crystallite size was calculated using the Debye-Scherrer formula:

$$D = \frac{k\lambda}{\beta Cos\,\theta} \quad (1)$$

Where k (shape factor) = 0.89, λ = the wavelength of the Cu-Kα radiations, β = the full width half maximum, and θ = angle derived from 2θ value of peak with maximum intensity in the XRD diffractogram.

Furthermore, the reducibility of the catalysts was investigated with H_2 temperature-programmed reduction (H_2-TPR) using a Micromeritics Autochem II. About 30 mg of the catalytic sample was loaded in a quartz tube reactor and pretreated under Argon flow at 200 °C for 1 h before each test. The material was probed by passing 10 % H_2/Ar through the catalyst bed at a flow rate of 50 mL min^{-1}. The measurements were performed within the range of 25−800 °C at 10 °C min^{-1} ramping rate.

2.4. Catalytic evaluation of prepared catalysts in Oppenauer oxidation of alcohols

The liquid phase Oppenauer oxidation experiments were performed on a carousel reaction station multi-reactor (Radley Discovery Technologies) having twelve 50 mL reaction vials. The substrate, acetone, and catalysts were added to the reaction vessel in the following proportion, substrate:catalyst amount 1:1 mass ratio, substrate:acetone 1:100 M ratio. The mixture with the required amount of decane as internal standard was heated with a stirring rate of 450 rpm using a 16.5 mm crossbar stirrer at a temperature of 50 °C. The agitation rate was chosen after a preliminary study. The upper part of the vial was kept at 5 °C using a temperature-controlled condenser to prevent the loss of acetone *via* evaporation.

The filtered liquid products were analyzed using a Shimadzu GC-2010 equipped with a flame ionization detector (FID), capillary column (Rxi-5Sil; 30 m, 0.2 mm ID, thickness 0.25 μm), and N_2 as the carrier gas. The injection port and FID temperatures were 200 °C and 350 °C, respectively. Also, on a Shimadzu GC–MS QP-2010 operating with similar capillary column and injection temperature. For both GC-FID and MS, the column oven temperature program started 40 °C (hold 2 min), then programmed at 20 °C min^{-1} to 280 °C (hold 5 min) resulting in 19 min analytical time (see details in SI pg. S11).

The process variables were optimized such as the concentration of benzyl alcohol, catalyst loading, reaction temperature, and time over pure zirconia. The optimized reaction conditions were followed in examining the activity of as-prepared M_ZrO_2, Pd/ZrO_2, and Pd/M_ZrO_2 catalysts. The recyclability tests were performed under optimized reaction conditions. The solid catalyst was separated by centrifugation, washed with acetone five times, and dried under a vacuum at 80 °C for 12 h before subsequent use. The substrate conversion and product selectivity of the catalysts were calculated (Eqs. 2 and 3).

$$\text{Conversion}\ (\%) = \frac{benzyl\ alcohol_t}{benzyl\ alcohol_{in}} \times 100 \quad (2)$$

$$\text{Selectivity}\ (\%) = \frac{product_{(x)}}{product_{(1)} + product_{(2)} + product_{(3)}} \times 100 \quad (3)$$

Where $benzyl\ alcohol_t$ = mol of benzyl alcohol at time t, $benzyl\ alcohol_{in}$ = initial mol of benzyl alcohol, $product_{(x)}$ = mol of (1) or (2) or (3) produced after time t, (1) = benzaldehyde, (2) = β-hydroxyketone, and (3) = benzylideneacetone.

3. Results

3.1. Acidity-basicity characterization of the as-synthesized ZrO_2 based catalysts

A significant change in the acid-base properties of ZrO_2 upon the incorporation of metal dopants and the loading of Pd nanoparticles was observed. The total acidity and basicity of the surface of the synthesized materials were determined through NH_3-TPD and CO_2-TPD experiments, respectively (Table 1). The peak area as shown in (Figs. 1a and S1) implies the acidic strength of the catalysts. A broad peak of ammonia desorption in the region of 109−283 °C was observed in all the

Table 1
The surface acidity and basicity of the as-synthesized ZrO_2 based catalysts.

Entry	Meso	Total acidity ($mmol_{NH3}\ g^{-1}$)	Total basicity ($mmol_{CO2}\ g^{-1}$)	Ratio (acidity/basicity)
1	ZrO_2	0.80	0.63	1.27
2	Ce_ZrO_2	0.38	1.43	0.27
3	Pd/Ce_ZrO_2	0.69	1.04	0.66
4	Pd/ZrO_2	0.42	0.36	1.17

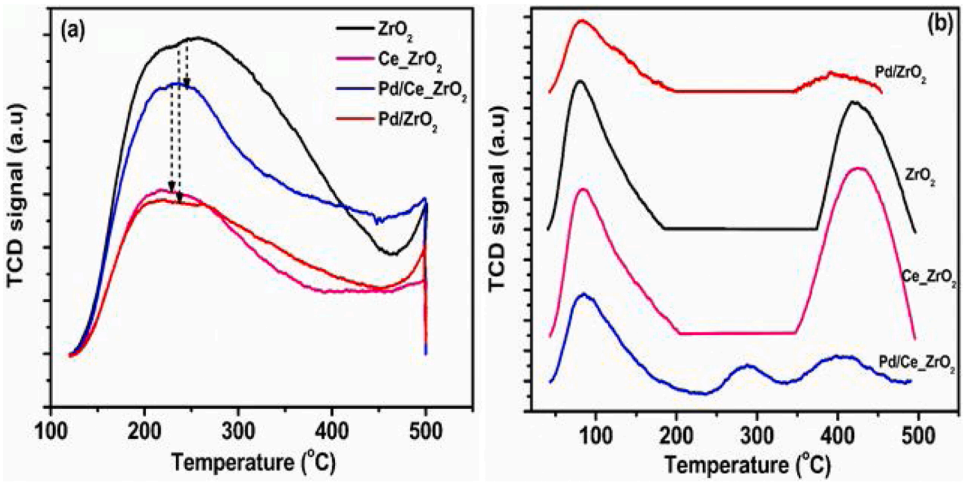

Fig. 1. (a) NH_3-TPD and (b) CO_2-TPD profiles of the as-synthesized mesoporous ZrO_2 based catalysts.

materials. This is an indication of weak and medium surface acidic sites. Also, a strong acidic site with a broad peak around 450 °C was observed in the Cr_ZrO_2 sample (Fig. S1). The Cr_ZrO_2 sample presented the highest total acidity of 1.11 $mmol_{NH3}$ g^{-1} (Table S1), which was higher than that of the pure ZrO_2 (0.80 $mmol_{NH3}$ g^{-1}) similar to previous studies [27]. The total acidity of the as-prepared catalysts is within the range of 0.38–1.11 $mmol_{NH3}$ g^{-1} (Table S1). The Ce_ZrO_2 sample showed the lowest amount of weak acidic sites 0.38 $mmol_{NH3}$ g^{-1} with a broad peak around 230 °C. However, there was a significant increase in the acid sites when Pd nanoparticles were supported on Ce_ZrO_2 but not as much as that of pure zirconia. In the case of Pd/ZrO_2, the total acidity of pure ZrO_2 was reduced by about 50 %, from 0.80−0.42 $mmol_{NH3}$ g^{-1} after the loading of Pd nanoparticles. Upon loading with Pd nanoparticles, the main peak shifted to lower temperatures. This could be ascribed to a partial blanketing of the ZrO_2 medium acidic sites by the Pd nanoparticles, generating weak acidic sites [27]. The NH_3-TPD profile of other synthesized mesoporous M_ZrO_2 as shown in Fig. S1 in the supplementary information suggests that the dopant-induced acidity decreases across the period.

The basic properties of all the mesoporous catalysts as revealed in (Table 1 and Fig. 1b) are a function of the synergistic metal-metal interaction [28]. The distribution of the basic sites over the surface of the catalysts showed two prominent peaks at 80 °C and 419 °C for ZrO_2; 78 °C and 376 °C for Pd/ZrO_2 representing both weak and strong basic sites, respectively. The shift to lower temperature observed in the CO_2 desorption peaks of Pd/ZrO_2 evidenced the formation of weaker basic sites on the catalyst's surface by the Pd nanoparticles and the reduced peak intensity signifies a reduction in the concentration of the basic sites. The results correlate well with the literature [29]. The surface base concentration of pure mesoporous ZrO_2 was 0.80 $mmol_{CO2}$ g^{-1}. However, a significant decrease in the concentration of the base sites to 0.36 $mmol_{CO2}$ g^{-1} was observed for Pd/ZrO_2. When the pure mesoporous ZrO_2 was doped with Ce, the concentration of the base sites significantly increased to 1.43 $mmol_{CO2}$ g^{-1}, showing a more prominent strong basic peak around 425 °C and a weak base around 84 °C. The two broad weak and strong basic peaks shifted to higher temperatures indicating generation of stronger basic sites upon the incorporation of Ce into the Zr matrix.

The higher amount of basic sites in Ce_ZrO_2 is attributed to the presence of Ce^{4+} which generates surface oxygen anions as basic sites in the catalyst [29]. When Pd nanoparticles were deposited on the Ce_ZrO_2 support, the distribution of the basic site over the surface of the Pd/Ce_ZrO_2 catalyst as shown by the CO_2-TPD experiments (Fig. 1b) presented three broad peaks representing weak, medium, and strong base sites around 85 °C, 287 °C and 402 °C, respectively. The generation of a new peak at 287 °C representing medium base sites in Pd/Ce_ZrO_2 could be attributed to the Pd-Ce interaction. The intensity of these peaks significantly decreased compared to that of the support Ce_ZrO_2. The basic site concentration on Ce_ZrO_2 decreased to 1.04 $mmol_{CO2}$ g^{-1} after the deposition of Pd nanoparticles. Nevertheless, the base concentration of Pd/Ce_ZrO_2 1.04 $mmol_{CO2}$ g^{-1} is higher than that of the pure ZrO_2 0.80 $mmol_{CO2}$ g^{-1} and Pd/ZrO_2 0.36 $mmol_{CO2}$ g^{-1}. It could be deduced that the interaction between Ce-Zr dominates that of other metal-metal interactions (Pd-Zr and Pd-Ce) in the case of the Pd/Ce_ZrO_2 catalyst.

The results of the NH_3-TPD and CO_2-TPD indicate that all the as-prepared catalysts possess both acidic and basic sites of different strengths. The influence of foreign atomic species in the framework of zirconia on its acidic and basic sites was evident. The acidic sites decreased upon the incorporation of metal species (Ce and Pd). However, basic sites depend on the kind of dominant metal-metal interaction. For instance, the catalysts containing Ce even in the presence of Pd gave more basic sites than that of pure ZrO_2, while the catalyst containing only Pd showed less basic sites. Also, it could be said that the strength of the adsorption sites depends on the kind of foreign metal specie and interaction with the host ZrO_2.

3.2. *Textural characterization of the as-synthesized mesoporous ZrO_2 based catalysts*

The transmission electron (TEM) images showed the morphology and the crystallinity of the prepared pure mesoporous ZrO_2 and ZrO_2 based catalysts (Figs. 2 and S2). In the case of ZrO_2, a porous structure was observed and the preservation of the pore structure upon deposition of Pd nanoparticles and addition of dopant is evident (Figs. 2c and S2 respectively). The Pd nanoparticles, with an average size of 6.5 ± 1.0 nm (Fig. 2e), are uniformly distributed on the host zirconia (Fig. 2c). Also, enhanced crystallinity upon deposition of Pd nanoparticles was observed (Fig. 2d), this supports the results from the pXRD analysis showing increased peak intensity compared to the host. The high-resolution electron micrograph indicates the distinct fringe patterns which confirmed the formation of single-phase ZrO_2 with the long-range order in the structure (Fig. 2d).

The scanning electron microscopy (SEM) images (Figs. 3 and S3) showed that there was no occurrence of microscopical structural change after the incorporation of metal dopants and deposition of Pd nanoparticles. The surface textural properties of ZrO_2 could be said to be stable upon the incorporation of another metal specie. The metal composition on the catalysts is also evidenced in the SEM-EDX and their corresponding weight percentage (Figs. 3c and S4c). The EDX elemental mapping (Figs. 3d, and S5) also indicate that the Pd nanoparticles are

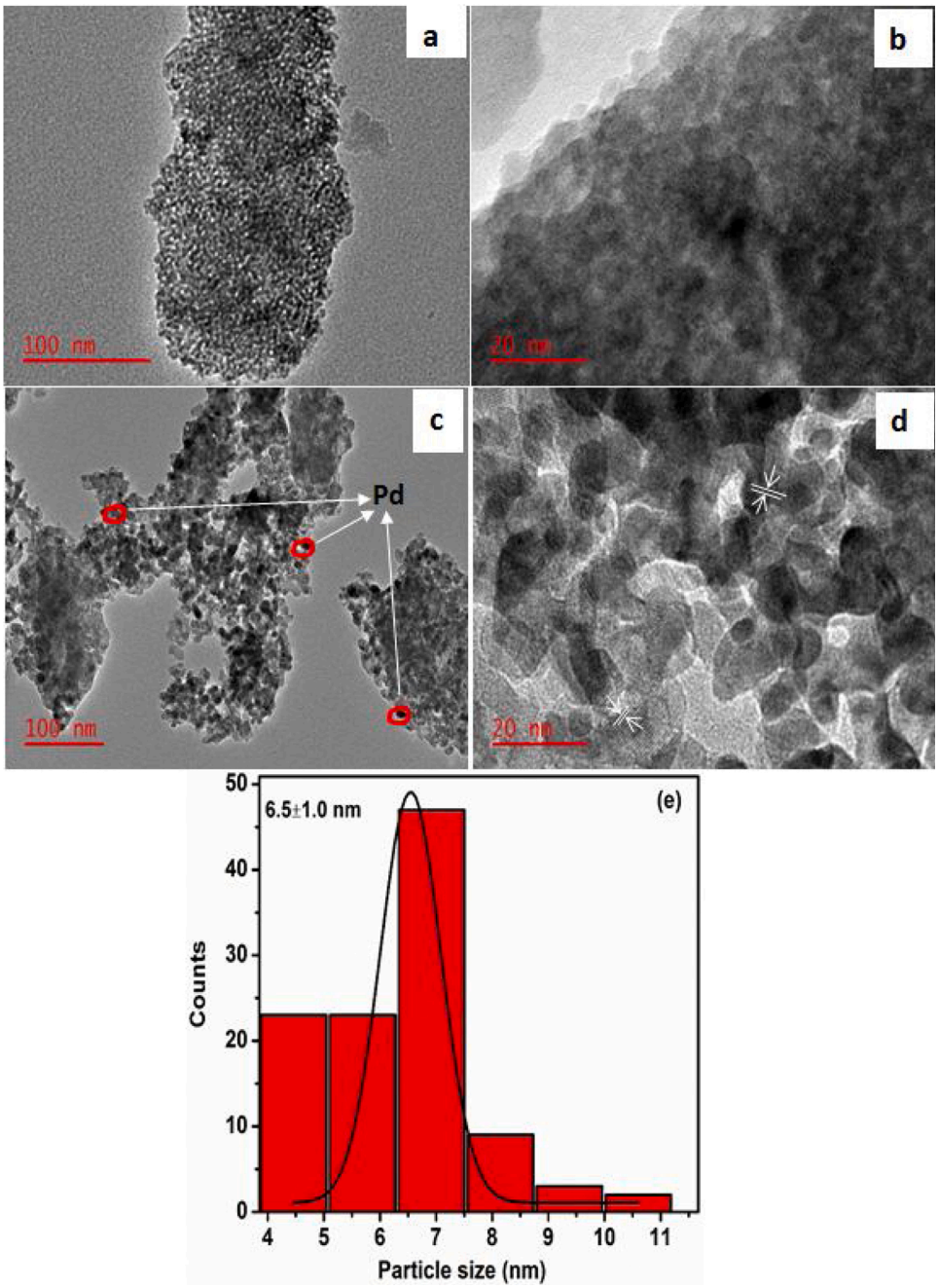

Fig. 2. TEM and HRTEM micrographs of (a and b) pure ZrO_2 and (c and d) Pd/ZrO_2 samples and (e) Pd nanoparticle size distribution histogram for Pd/ZrO_2 (200 particles counted at 100 nm scale bar).

well dispersed on the ZrO_2 matrix due to strong interaction between the Pd-Zr.

Furthermore, the nitrogen sorption analysis revealed that the catalysts exhibited high surface area S_{BET} and mesopores with Type IV isotherms. The presence of foreign atomic species alters the structural properties of the host ZrO_2 (Tables 2 and S2). The BET surface area of the host zirconia (206 $m^2\ g^{-1}$) increased upon doping with Mn (221 $m^2\ g^{-1}$) and Fe (223 $m^2\ g^{-1}$). The surface area decreased in the presence of Cr (193 $m^2\ g^{-1}$), Ni (193 $m^2\ g^{-1}$), and Ce (145 $m^2\ g^{-1}$). The deposition of Pd NPs also reduced the S_{BET} of the supports with a drastic reduction from 205 $m^2\ g^{-1}$-73 $m^2\ g^{-1}$ in the case of Pd/ZrO_2 and 145 $m^2\ g^{-1}$-132 $m^2\ g^{-1}$ in Pd/Ce_ZrO_2. Enlargement of the pore diameter from 2.58 to 3.63 nm upon the incorporation of metal dopants and deposition of Pd nanoparticles on ZrO_2 occurred (Table 2, Figs. 4b, and S6c). Besides, doping with a metal resulted in the pore volume stability and enhancement from 0.10-0.26 $cm^3\ g^{-1}$ whereas a slight decrease was found when Pd nanoparticles were immobilized on the ZrO_2 and Ce_ZrO_2 support. These suggest that the Pd nanoparticles are well embedded in the ZrO_2 support. The isotherms of all the catalysts (Figs. 4 and S6a and b) are typical of Type IV according to the IUPAC classification [30,31] which is a characteristic feature of mesoporous materials. The preservation of the pore network after metal incorporation was also indicated in the TEM micrographs (Figs. 2 and S2).

The XRD diffractograms (Figs. 5 and S7) reveal the fact that ZrO_2 nanoparticles with tetragonal symmetry were formed. The tetragonal phase corresponding to JCPDS Card No. 79-1771 was indexed at peaks 30.4° (101), 35.3° (110), 50.7° (112), 60° (211), 63.1° (202), 74.8° (220). This is similar to previously reported results [32,33]. The intense

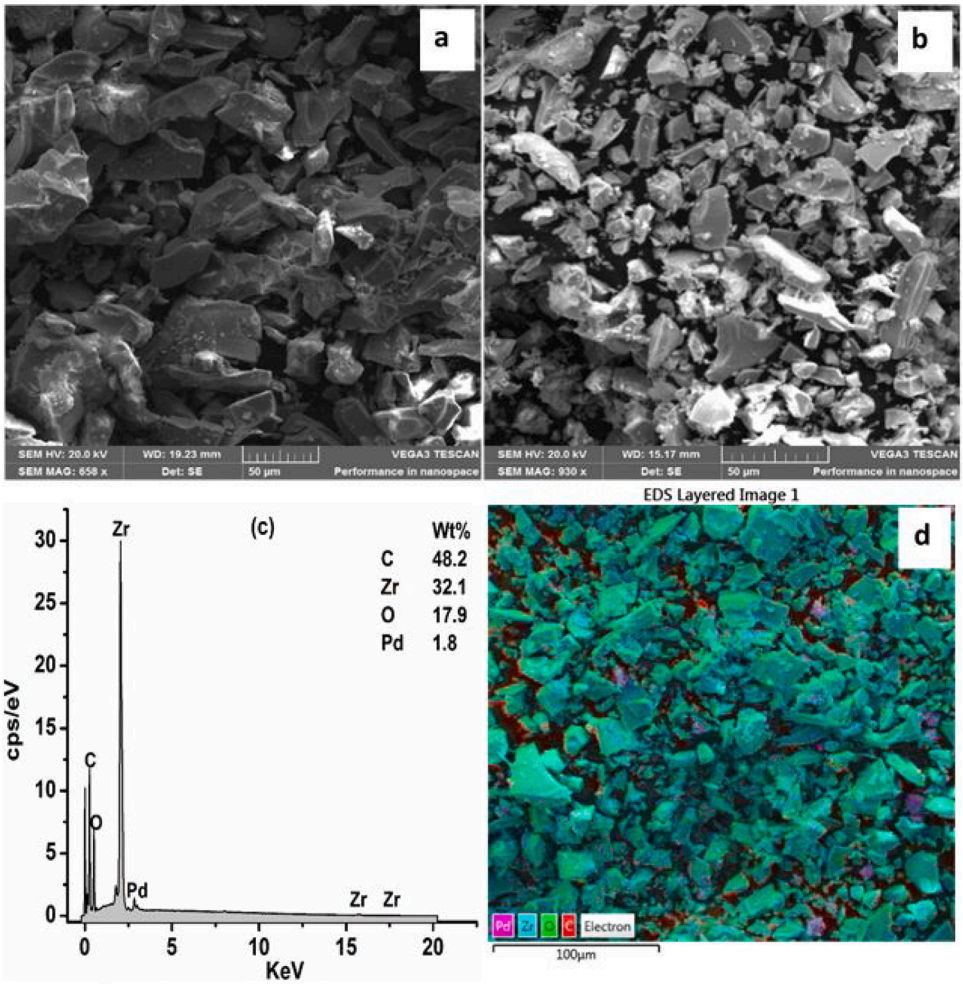

Fig. 3. SEM image (a) pure ZrO_2, (b) Pd/ZrO_2; EDX (c) Pd/ZrO_2 and EDX elemental maps (d) Pd/ZrO_2 respectively.

Table 2
The structural properties of the synthesized mesoporous ZrO_2 based catalysts.

Entry	Meso	Pd content (wt%)		S_{BET} (m^2 g^{-1})	Pore diameter (nm)	Pore volume (cm^3 g^{-1})	Crystallite[c] size (nm)	Crystal structure
		a	b					
1	ZrO_2	–	–	206	2.58	0.10	5.32	Tetragonal
2	Ce_ZrO_2	–	–	145	2.91	0.11	1.87	Tetragonal
3	Pd/Ce_ZrO_2	0.60	1.10	132	2.89	0.09	8.83	Tetragonal
4	Pd/ZrO_2	1.79	1.80	73	3.59	0.08	8.86	Tetragonal

Pd content determined by ICP-OES = a, EDX = b, BET surface area = S_{BET}. Crystallite size = c, calculated using Debye-Scherrer formula (Eq. 1).

XRD lines observed for the doped ZrO_2 (Fig. 5a) are broader, which can be attributed to the lattice distortion of the tetragonal phase of ZrO_2 caused by the incorporation of cation dopant. However, the reflections in the case of Ni and Cr significantly disappeared, an indication of the amorphous phase [34]. The absence of reflections of the Pd nanoparticles phase could be due to the low Pd percentage loading which is below the detection limit of the diffractometer. More so, it depicts that the Pd species are well dispersed on the ZrO_2. Meanwhile, the TEM, EDX, and SEM mapping further confirmed the presence of Pd nanoparticles. The Pd supported catalysts showed higher crystallinity compared to the pure ZrO_2 and other M_ZrO_2 evidenced in the calculated crystallite size shown in Table 2 and the increased peak intensity (Fig. 5b). Increased peak intensities depict enhanced crystallinity which could be ascribed to the improvement in the structural arrangement of the ZrO_2 framework upon deposition of Pd nanoparticles. This phenomenon also explains the occurrence of enlargement of pore and widened isotherm (Fig. 4). The tetragonal phase of zirconia was modulated upon doping with transition metals and after loading of Pd nanoparticles.

3.3. *Reducibility characterization of ZrO_2, M_ZrO_2, and Pd/ZrO_2 catalysts*

The redox properties of the as-synthesized Zr-based catalysts were examined using H_2-TPR analysis and the profiles of the catalysts are presented in (Figs. 6 and S8). There was no significant peak in the profile of the pure ZrO_2. This is typical of non-reducible oxide [29]. The interaction between Zr and the transition metal dopant enhances the reducibility of ZrO_2 (Fig. S8). The Cr dopant in correlation with others showed the lowest temperature reduction peak at 260 °C ascribed to the reduction of bulk oxygen (Fig. S8). The presence of Pd tends to improve the reducibility of the pure ZrO_2, this is confirmed by the appearance of a broad reduction peak at 518 °C (Fig. 6). The broad peak at 518 °C

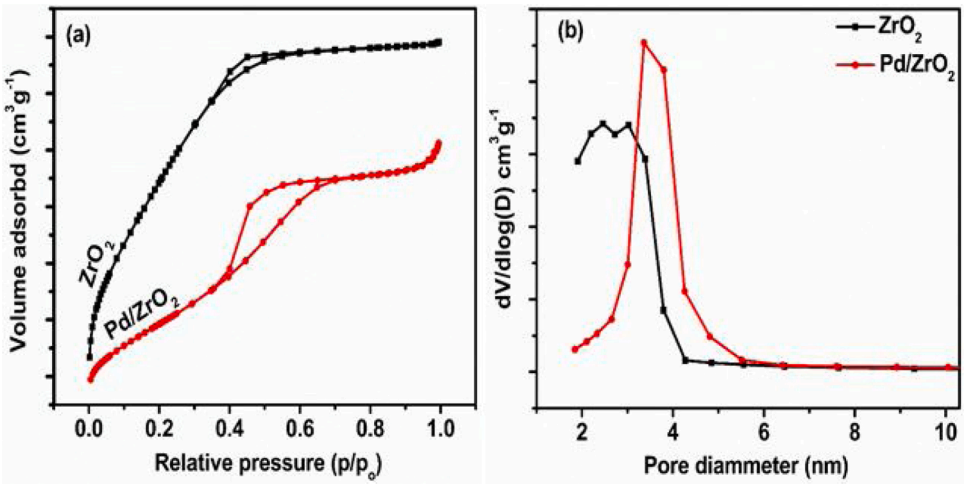

Fig. 4. (a) N_2 adsorption-desorption isotherms (b) pore size distribution of pure ZrO_2 and Pd/ZrO_2.

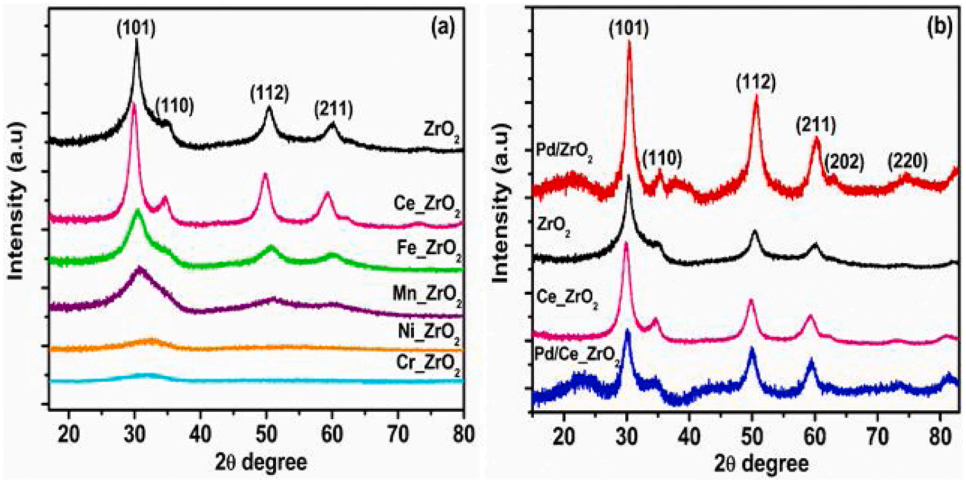

Fig. 5. Comparison of wide-angle powder XRD of (a) pure ZrO_2 and M_ZrO_2 (b) Pd/M_ZrO_2 patterns.

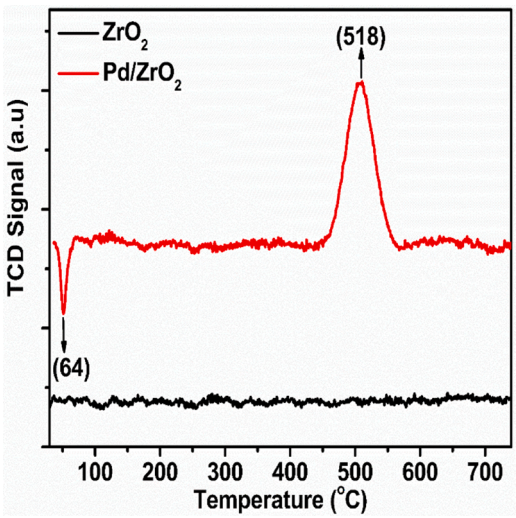

Fig. 6. H_2-TPR profiles of mesoporous pure ZrO_2 and (b) Pd/ZrO_2.

evidenced the strong Pd-Zr interaction. Besides, it could be explained that the reducibility of the ZrO_2 support is made possible by the H_2-spillover from metallic Pd, a similar phenomenon was reported by Wang et al. [35] Also, the Pd/ZrO_2 catalyst has a negative peak at 64 °C indicating the presence of metallic Pd. In H_2-TPR, Pd metal tends to absorb a considerable amount of H_2 at low temperature and subsequently; releases the adsorbed hydrogen with increase temperature [35].

3.4. Catalytic evaluation of prepared catalysts in Oppenauer oxidation of alcohol

The selective Oppenauer oxidation of benzyl alcohol over pure ZrO_2 was used as the model reaction. The reaction was significantly influenced by different process conditions such as the catalyst loading, concentration of benzyl alcohol, reaction temperature, and time. There was no significant product formed from the blank experiment after 24 h. The reaction parameters were optimized using an undoped ZrO_2 catalyst.

3.4.1. The amount of benzyl alcohol converted is limited by the surface active site on the catalyst

A benzyl alcohol concentration in the range of 1.0–3.0 mmol was utilized in the catalytic reaction and shown in Figs. 7a and S9a. The rate of agitation was maintained at 450 rpm at 50 °C using 0.10 g of the prepared ZrO_2 catalyst. There was not much influence of increasing the concentration of benzyl alcohol on the amount converted. The amount converted after 8 h remains approximately constant (~ 0.70 mmol) when the concentration of benzyl alcohol in the catalytic system was

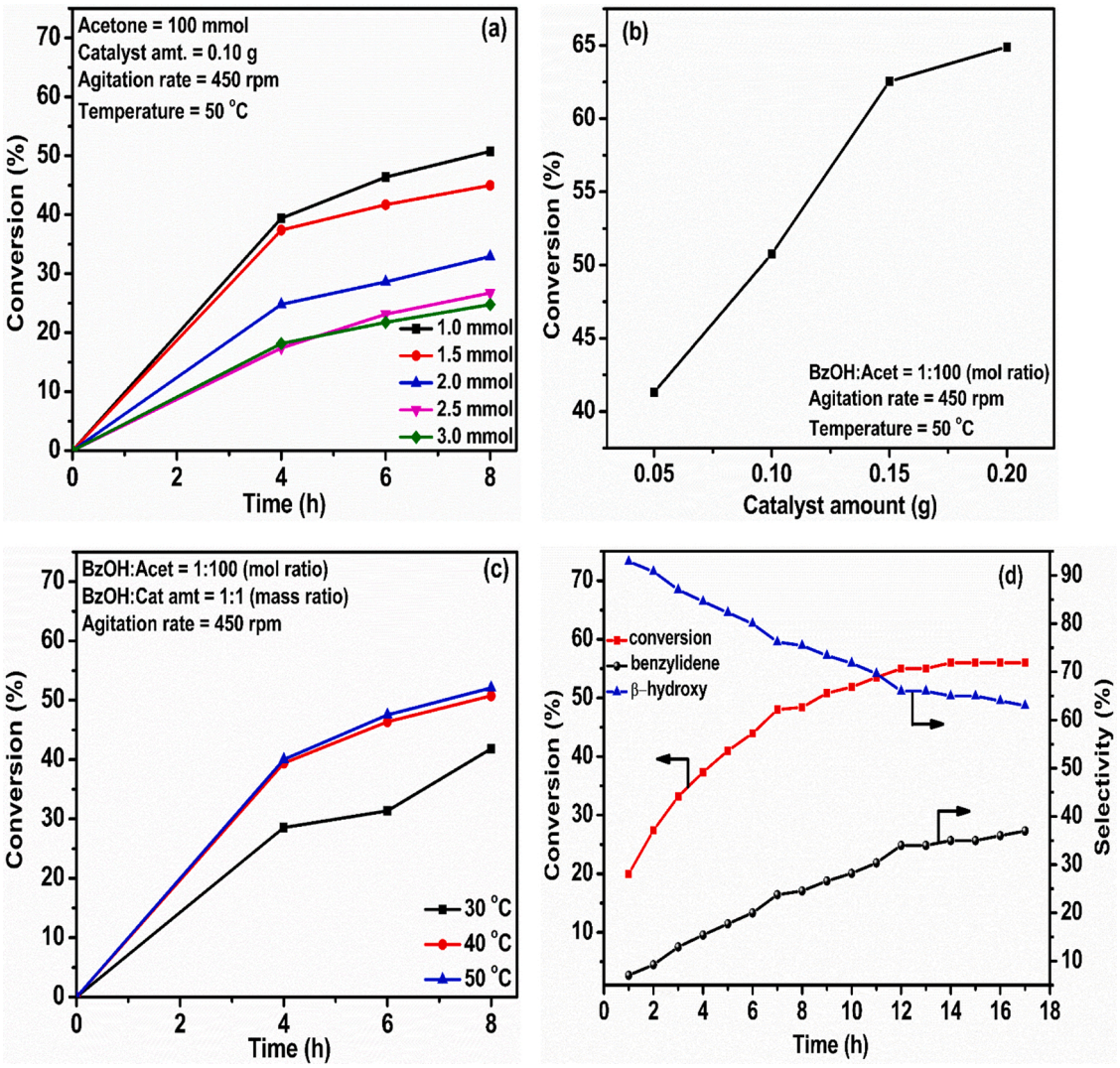

Fig. 7. Effect of (a) concentration of benzyl alcohol (b) catalyst loading (c) temperature and (d) reaction time on the catalytic activity of ZrO_2 in the Oppenauer oxidation of benzyl alcohol.

increased above 1.5 mmol. The indicates that in this system, a similar amount of substrate was converted in each experiment. The amount of benzyl alcohol molecules converted per time is limited to the available surface active phase on the ZrO_2 catalyst. This could be due to over-saturation of the catalyst active sites, which possibly hinder uniform migration of the benzyl alcohol molecules over the catalyst surface, leading to a surface reaction where there is competitive adsorption for reactive sites. A concentration of 1.0 mmol benzyl alcohol was chosen for the subsequent reactions. The reaction performed using toluene in addition to acetone gave about a 50 % decrease in conversion. This implies that the ZrO_2 catalyst is fairly active in the presence of toluene. A 100-molar equivalent of acetone only was used for the subsequent reactions.

3.4.2. *The reactivity increases with catalyst amount*

The effect of the amount of catalyst was investigated in the domain of 0.05–0.20 g with other variables kept constant. It is observed in Figs. 7b and S9b that the reactivity increased with increasing catalyst amount as expected. The activity could be attributed to increased active sites on the catalyst's surface. A further indication of surface reaction. Moreover, the kinetic control regime that is, a linear relationship lies between the varied catalyst amount. Any of the amount used could be chosen as the optimum amount hence, 0.10 g was chosen for the subsequent Oppenauer experiments. This experimental data confirm the trend observed in the variation of concentration of benzyl alcohol with the absolute amount converted (Fig. S9c), that the catalytic activity in this system is governed by the active sites available for reaction within the surface coverage of the catalyst.

3.4.3. *Dependence of catalytic reactivity on temperature*

The relationship between the reaction temperature and the catalyst reactivity is shown in Fig. 7c. As expected, the activity of ZrO_2 in Oppenauer oxidation of benzyl alcohol increased with increasing reaction temperature. This explains the fact that the Oppenauer reaction is kinetically driven. The temperature effect on the prepared catalysts' performance and selectivity to the desired products was investigated, varying the temperature from 30 to 50 °C. Irrespective of the temperature used, aldol products were formed over pure ZrO_2. However, selectivity to benzylideneacetone increased with increasing temperature. The reaction temperature of the subsequent experiments was limited to 50 °C considering the boiling point of acetone.

3.4.4. *The products distribution as the reaction time progresses*

As shown in the time variation study Fig. 7d, the catalytic activity increased with time and was found to be approximately constant beyond 14 h reaction time. At 50 °C, a considerable conversion of 56 % was

attained after 14 h. The selectivity for the products varied as the reaction time progresses. The selectivity for β-hydroxyketone drastically decreased from 93−63% while that for benzylideneacetone appreciably increased over time from 7 to 37%. However, the target product benzaldehyde was not detected over ZrO_2. This could be due to over oxidation or consumption of the benzaldehyde in aldol condensation with acetone (Scheme 2).

3.5. Synergistic effect of M-Zr vs Pd-Zr interaction on product distribution

The activity of the Zr containing catalysts were examined in the Oppenauer oxidation of benzyl alcohol at 50 °C for 8 h. The effect of modification of zirconia *via* doping with transition metals or immobilization of Pd nanoparticles was significant in the reaction pathway determining the product distribution (Table 2, Table S3, Scheme 2, and Fig. 8a). The Cr doped zirconia presented no activity due to a larger amount of acid sites than that of the host (Table S3). Upon doping with Mn, Fe, Ni, and Ce, the Oppenauer oxidation spontaneously extends to aldol condensation of acetone with the synthesized benzaldehyde (Step 1B, Scheme 2). The Mn, Fe, and Ni-doped ZrO_2 were selective to intermediate product β-hydroxyketone of the aldol addition. However, over Ce-ZrO_2 and pure ZrO_2, the reaction proceeded to the final product benzylideneacetone. Komanoya et al. [36] showed from their experiments that ZrO_2 has large amounts of basic sites. We further showed by testing a pure CeO_2 with basic sites concentration of 2.28 μmol m^{-2}, higher than that of pure ZrO_2 (0.73 μmol m^{-2}) as shown by the CO_2-TPD in the reaction, that the two aldol products were formed with a higher yield (Table S3). Therefore, we conclude that basic sites are responsible for the synthesis of aldol products.

Interestingly, upon immobilization of Pd nanoparticles, 100 % selectivity to benzaldehyde was observed. The Pd-Zr interface modifies the electronic properties of zirconia as evidenced by the H_2-TPR experiment (Fig. 6). The Oppenauer oxidation terminates after the benzaldehyde synthesis without an extension to the aldol condensation pathway thus, enhancing the selectivity of the system for the production of benzaldehyde (Step 1A, Scheme 2). Also, it could be said that the presence of Pd nanoparticles governs the adsorption sites. It facilitates the moderation of the amount of Lewis acid and base sites for the selectivity to benzaldehyde (Figs. 8b and S9d). Moderate Lewis acid-base sites are essential to facilitate a synergy between the Lewis acidic and basic sites, which are required for tuning the selectivity towards benzaldehyde. The observed results may not be comparable with literature as related catalytic study in the oxidation of benzyl alcohol in acetone is rare in literature.

However, an aldol condensation product β-hydroxyketone was formed alongside benzaldehyde in the case of Pd/Ce_ZrO_2, as shown in Table 3 and Fig. 8a. This is attributed to the dominating basic sites as a result of Ce-Zr interface synergy as depicted in Table 1 and Fig. 8b, with the Ce-Zr catalyst showing the highest concentration of basic sites (Fig. S9d). It could be deduced from the results summarized in Figs. 8b and S9d that, moderate basicity and acidity is the major factor governing selectivity to benzaldehyde in the Oppenauer oxidation of benzyl alcohol with acetone in the proposed catalytic system. Therefore, tailoring the surface acid-base adsorption sites of the catalytic system is worthwhile.

3.6. Stability and reusability of Pd/ZrO_2

The ability of heterogeneous catalysts to retain their activity and selectivity after many reaction cycles portray the stability and sustainability of such a catalyst. Fig. 9 presents the data from the stability and reusability studies of Pd/ZrO_2 for the Oppenauer oxidation of benzyl alcohol to benzaldehyde. The reactivity of Pd/ZrO_2 shows that the catalyst has good stability for the subject reaction. The first catalytic run gave 43 % benzyl alcohol conversion and 98 % benzaldehyde selectivity. Thereafter, the selectivity to benzaldehyde increased to 100 % and was retained throughout the subsequent reuse. However, after eight consecutive catalytic cycles, the efficacy of the Pd/ZrO_2 catalyst declined, this could be ascribed to the reduction in the amount of the catalyst in the system due to loss during washing, before the next catalytic cycle.

4. Discussion

The most important role of a catalyst is to favor the selectivity for the most desired product in a multi-product reaction even at the expense of the catalytic activity that is, substrate conversion [37]. In this case, tunability of the product distribution in Oppenauer oxidation of benzyl alcohol in acetone is achieved upon modification of zirconia with metals. Enhanced selectivity to benzaldehyde was obtained over Pd/ZrO_2. We propose that the Pd-Zr intermetallic alloy site is responsible for the enhanced selectivity. This hypothesis was supported by

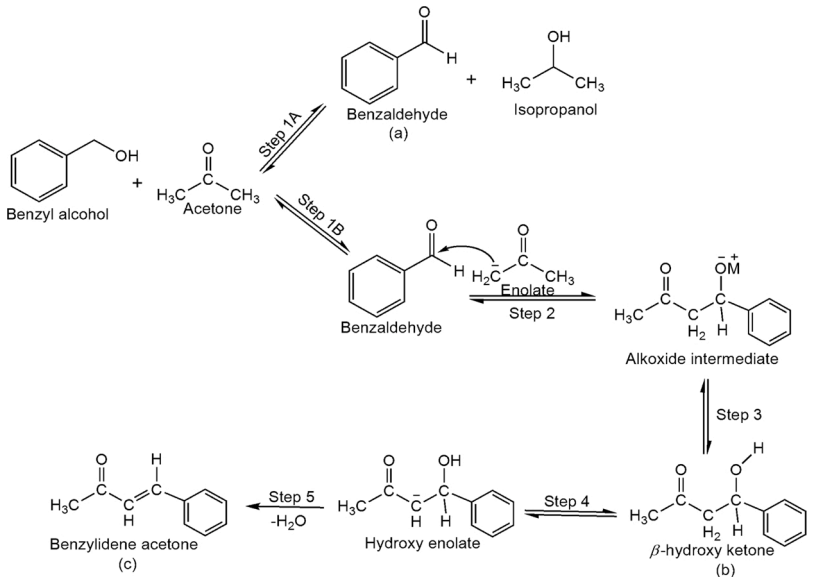

Scheme 2. Illustrative schematic diagram of the possible reaction pathways: Step IA (Oppenauer oxidation of benzyl alcohol) and Step 1B (aldol condensation of acetone).

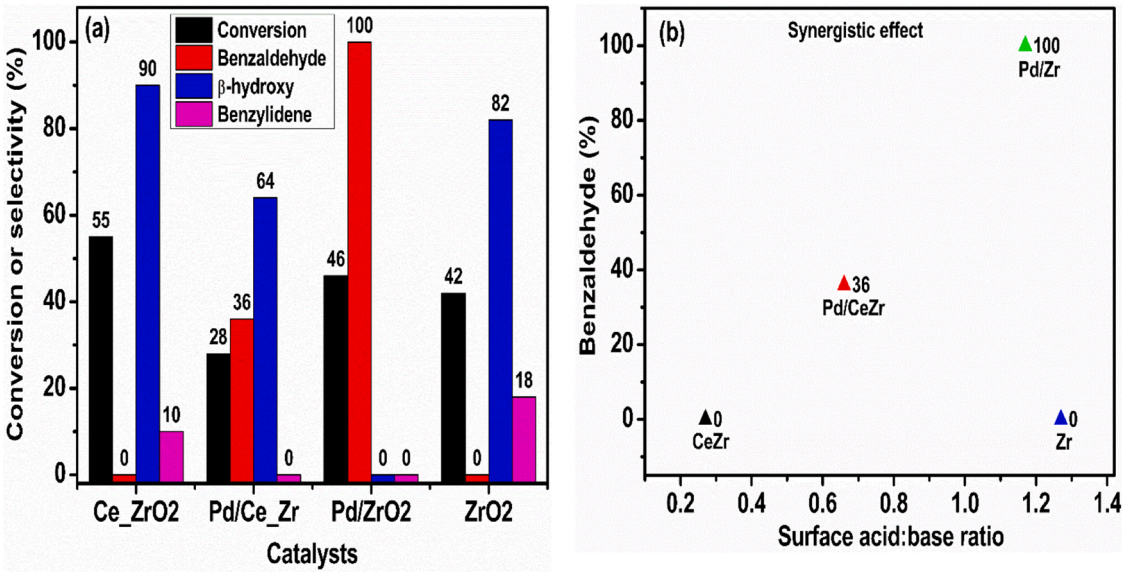

Fig. 8. (a) Distribution of products and conversion of benzyl alcohol using acetone as H-donor over Zr-based catalysts (b) influence of surface acid:base ratio on selectivity for benzaldehyde as a function of metal-Zr synergy.

Table 3
Comparison of the S_{BET} and activity of the mesoporous zirconia-based catalysts.

Entry	Catalyst	S_{BET} ($m^2\ g^{-1}$)	Specific activity* ($m^{-2}g$) × 10^{-3}	Conversion (%)	Selectivity (%)		
					(a)	(b)	(c)
1	ZrO_2	206	204	42	0	82	18
2	Cr_ZrO_2	190	0	0	0	0	0
3	Mn_ZrO_2	221	24	5	0	100	0
4	Fe_ZrO_2	223	117	26	0	100	0
5	Ni_ZrO_2	193	80	15	0	100	0
6	Ce_ZrO_2	145	378	55	0	90	10
7	Pd/Ce_ZrO_2	132	213	28	36	64	0
8	Pd/ZrO_2	73	630	46	100	0	0
9	Pd/SiO_2	–	–	2	100	0	0

Products: (a) Benzaldehyde, (b) β-hydroxyketone, (c) benzylideneacetone.
Reaction condition: acetone:benzyl alcohol = 100 M ratio, 1.0 mmol decane, 0.10 g catalyst, stirring rate 450 rpm, temperature 50 °C for 8 h.
* Specific activity (m^{-2} g) = conversion normalized by S_{BET}.

employing Pd supported on neutral SiO_2 support in the Oppenauer process, 100 % selectivity to benzaldehyde was obtained but with modest activity. Therefore, the synergy between Pd-Zr is responsible for both reasonable activity and selectivity to benzaldehyde. Komanoya et al. [36] in their experiments showed that the metal center acts as a Lewis acid site and facilitates the formation of a six-membered ring transition state with alcohol and ketone to accomplish the hydride transfer. The Pd nanoparticles moderate the concentration of Lewis acidic sites, this is also in agreement with the report of Gilkey et al. [38] that Lewis acid sites favor hydrogen transfer from alcohols to carbonyl groups through a six-member transition state. Therefore, the Pd-ZrO_2 interface served as the active site for benzyl alcohol Oppenauer oxidation to benzaldehyde and prevents further aldol condensation between the benzaldehyde and the acetone.

Moreover, the abstraction of hydrogen from the benzyl alcohol occurred at the active Pd sites. The electronic environment as evidenced by the H_2-TPR (Fig. 6) suggests the Pd particle sites favor H-transfer, the critical contributor to the significant promoting effect of Pd on the selectivity for benzaldehyde. Chan-Thaw et al. [39] stated that the deposition of Pd on a basic metal oxide facilitates H-abstraction from the O-H. The Pd-induced hydrogen transferred from the O-H was available for the reduction of the C = O of the acetone *via* a six-membered cyclic transition state (Scheme 1). Subsequently, isopropanol is formed, and the benzyl alcohol converted to benzaldehyde (Step 1A, Scheme 2). The synergy between ZrO_2 and the Pd-Zr intermetallic alloy is advantageous for benzaldehyde synthesis. The surface modification with Pd mediates improved selectivity to benzaldehyde in the Oppenauer oxidation of benzyl alcohol.

On the other hand, pure ZrO_2 with more acidic:basic sites in the presence of excess acetone activates the acetone to form an enolate which recombines with the product benzaldehyde to form hydroxylenolate and upon further hydration formed an aldol condensation product (Step 1B, Scheme 2). To achieve the synthesis of benzaldehyde, a synergy between almost equivalent Lewis acid and base sites on the catalyst is required (Fig. 8a and b). Also, catalysts with high Lewis base: acid concentration are selective to aldol products (β-hydroxyketone and benzylideneacetone) while those with excess Lewis acid:base concentration such as Cr_ZrO_2 (Table S1) were not active in either of the two possible reaction pathways (Oppenauer oxidation and aldol condensation). Oppenauer oxidation *via* the six-membered cyclic transition was achieved over active Pd supported zirconia catalyst with a moderate concentration of Lewis acidic-basic sites (Table 1 and Fig. 8a and b).

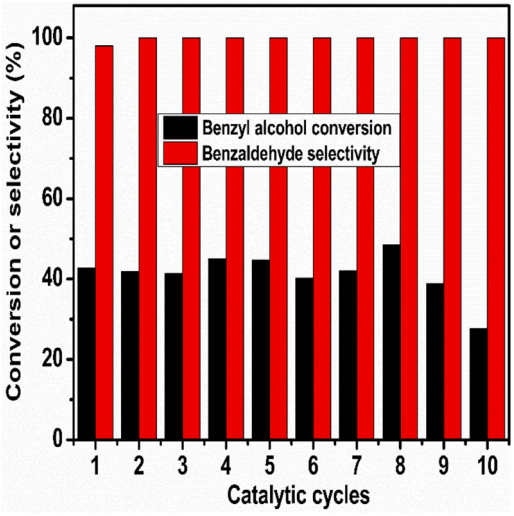

Fig. 9. Catalytic stability and reusability test of Pd/ZrO_2. The solid was vacuum dried at 80 °C for 12 h before each reaction. The same reaction conditions indicated in Table 3 were used in these catalytic runs except the reaction time, 6 h.

5. Conclusions

A successful synthesis of mesoporous cation modified zirconia and Pd supported zirconia-based catalysts is reported. The structural properties of the catalyst are dependent on the nature of component species. The appropriate integration of physicochemical properties of a multicomponent catalyst such as crystallinity, acidity, and basicity was exploited in tailoring the catalytic selectivity. In our case, the highly improved intrinsic properties of pure ZrO_2 by the deposited Pd nanoparticles cooperatively facilitate the enhanced selectivity of the target product benzaldehyde. For instance, the highly increased crystallinity supported the uniform dispersion of the Pd NPs and proper substrate orientation or alignment for rapid activation, and the moderation of Lewis acid-base sites directed the course of the reaction route *via* the six-membered cyclic transition state for the production of benzaldehyde and isopropanol. Interactions between the Lewis acid-base sites of similar concentration and reactants in Oppenauer oxidation of benzyl alcohol resulted in the selectivity modulation for the aldehyde product. The Pd-Zr sites are responsible for the generation of acid-base pair sites that suppress the aldol condensation pathway. The Pd/ZrO_2 catalyst is reusable keeping excellent 100 % selectivity to benzaldehyde after ten times. This work offers insight into understanding the structure-reactivity and development of active bifunctional catalysts by tuning the surface acid-base properties towards enhanced selectivity to the target product. Achieving optimum selectivity is crucial, as it is one of the means of achieving the goals of a sustainable chemical process. The investigation of the effect of Pd loading on catalytic activity is underway.

CRediT authorship contribution statement

Christianah Aarinola Akinnawo: Investigation, Data curation, Writing - original draft. **Dimakatso Jeannett Maheso:** Investigation. **Ndzondelelo Bingwa:** Conceptualization, Methodology, Writing - review & editing, Supervision. **Reinout Meijboom:** Conceptualization, Funding acquisition, Methodology, Project administration, Supervision, Writing - review & editing.

Declaration of Competing Interest

The authors report no declarations of interest.

Acknowledgments

The authors acknowledge the National Research Foundation of South Africa: NRF/TWAS UID: 105463, NRF UID: 117997, 85386, and 85364, and the University of Johannesburg for financial assistance. Also, the Spectrum division of the University of Johannesburg and Shimadzu, South Africa for their analytical instruments.

Appendix A. Supplementary data

Supplementary material related to this article can be found, in the online version, at doi:https://doi.org/10.1016/j.apcata.2021.118022.

References

[1] C.S. Ramirez-Barria, M. Isaacs, C. Parlett, K. Wilson, A. Guerrero-Ruiz, I. Rodríguez-Ramos, Catal. Today (2019).
[2] M.E. Assal, M. Kuniyil, M. Khan, M.R. Shaik, A. Al-Warthan, M.R.H. Siddiqui, J. P. Labis, S.F. Adil, Adv. Mater. Sci. Eng. 2017 (2017).
[3] R. Naik, A. Nizam, A. Siddekha, M.A. Pasha, Ultrason. Sonochem. 18 (2011) 1124–1127.
[4] M.B. Smith, J. March, March's Advanced Organic Chemistry: Reactions, Mechanisms, and Structure, John Wiley & Sons, 2007.
[5] G. Zhan, Y. Hong, V.T. Mbah, J. Huang, A.-R. Ibrahim, M. Du, Q. Li, Appl. Catal. A Gen. 439 (2012) 179–186.
[6] D.I. Enache, J.K. Edwards, P. Landon, B. Solsona-Espriu, A.F. Carley, A.A. Herzing, M. Watanabe, C.J. Kiely, D.W. Knight, G.J. Hutchings, Science (80) 311 (2006) 362–365.
[7] G.J. ten Brink, I.W.C.E. Arends, R.A. Sheldon, Science (80) 287 (2000) 1636–1639.
[8] T. Ooi, H. Otsuka, T. Miura, H. Ichikawa, K. Maruoka, Org. Lett. 4 (2002) 2669–2672.
[9] R. Chorghade, C. Battilocchio, J.M. Hawkins, S.V. Ley, Org. Lett. 15 (2013) 5698–5701.
[10] E. Baráth, Catalysts 8 (2018) 671.
[11] F. Alonso, P. Riente, M. Yus, Tetrahedron 65 (2009) 10637–10643.
[12] S. Gauthier, R. Scopelliti, K. Severin, Organometallics 23 (2004) 3769–3771.
[13] F. Gonell, M. Boronat, A. Corma, Catal. Sci. Technol. 7 (2017) 2865–2873.
[14] M. Boronat, A. Corma, M. Renz, J. Phys. Chem. B 110 (2006) 21168–21174.
[15] S.H. Liu, G.K. Chuah, S. Jaenicke, J. Mol. Catal. A Chem. 220 (2004) 267–274.
[16] F. Stavale, X. Shao, N. Nilius, H.-J. Freund, S. Prada, L. Giordano, G. Pacchioni, J. Am. Chem. Soc. 134 (2012) 11380–11383.
[17] T.W. van Deelen, C.H. Mejía, K.P. de Jong, Nat. Catal. (2019) 1–16.
[18] Y. Zhou, C. Jin, Y. Li, W. Shen, Nano Today 20 (2018) 101–120.
[19] Y. Li, J. Huang, X. Hu, F.L.-Y. Lam, W. Wang, R. Luque, J. Mol. Catal. A Chem. 425 (2016) 61–67.
[20] L. Wang, L. Zhu, N. Bing, L. Wang, J. Phys. Chem. Solids 107 (2017) 125–130.
[21] C.M.A. Parlett, D.W. Bruce, N.S. Hondow, A.F. Lee, K. Wilson, ACS Catal. 1 (2011) 636–640.
[22] C. Wen, Y. Wei, D. Tang, B. Sa, T. Zhang, C. Chen, Sci. Rep. 7 (2017) 1–11.
[23] V. Polshettiwar, R.S. Varma, Green Chem. 12 (2010) 743–754.
[24] L.J. Durndell, C.M.A. Parlett, N.S. Hondow, M.A. Isaacs, K. Wilson, A.F. Lee, Sci. Rep. 5 (2015) 9425.
[25] S. Upadhyay, Paripex-Indian J. Res. 8 (2019).
[26] C.A. Akinnawo, N. Bingwa, R. Meijboom, Catal. Commun. (2020) 106115–106120.
[27] Z. Xie, Y. Ren, J. Li, Z. Zhao, X. Fan, B. Liu, W. Song, L. Kong, X. Xiao, J. Liu, J. Catal. 372 (2019) 206–216.
[28] W. Bing, M. Wei, J. Solid State Chem. 269 (2019) 184–194.
[29] Y. Li, L. Wang, R. Yan, J. Han, S. Zhang, Catal. Sci. Technol. 5 (2015) 3682–3692.
[30] M. Thommes, K. Kaneko, A. V Neimark, J.P. Olivier, F. Rodriguez-reinoso, J. Rouquerol, K.S.W. Sing, (2015).
[31] M. Thommes, Chemie Ing. Tech. 82 (2010) 1059–1073.
[32] M. Kumaresan, K.V. Anand, K. Govindaraju, S. Tamilselvan, V.G. Kumar, Microb. Pathog. 124 (2018) 311–315.
[33] R. Dwivedi, A. Maurya, A. Verma, R. Prasad, K.S. Bartwal, J. Alloys Compd. 509 (2011) 6848–6851.
[34] X. Zhang, G. Cui, H. Feng, L. Chen, H. Wang, B. Wang, X. Zhang, L. Zheng, S. Hong, M. Wei, Nat. Commun. 10 (2019) 1–12.
[35] W. Wang, F. Yuan, X. Niu, Y. Zhu, Sci. Rep. 6 (2016) 19511.
[36] T. Komanoya, K. Nakajima, M. Kitano, M. Hara, J. Phys. Chem. C 119 (2015) 26540–26546.
[37] J.C. Védrine, ChemSusChem 12 (2019) 577–588.
[38] M.J. Gilkey, B. Xu, ACS Catal. 6 (2016) 1420–1436.
[39] C. Chan-Thaw, A. Savara, A. Villa, Catalysts 8 (2018) 431.